

Green-Gauss/Weighted-Least-Squares Hybrid Gradient Reconstruction for Arbitrary Polyhedra Unstructured Grids

Eiji Shima,^{*} Keiichi Kitamura[†] and Takanori Haga[‡]
Japan Aerospace Exploration Agency (JAXA), Sagamihara, Kanagawa 252-5210, Japan

I. Introduction

THE gradient calculation for reconstruction of dependent variables is one of critical issues for accuracy and robustness of computational fluid dynamics (CFD) methods. There are many choices for the reconstruction for arbitrary polyhedra or polygons in unstructured meshes [1-4], represented by a family of weighted-least-squares (WLSQ) methods [including unweighted least-squares (LSQ)] and a Green-Gauss (G-G) method. The WLSQ methods give exact gradients for a linear distribution of the variables. On the other hand, the G-G reconstruction has this property only on symmetric and uniform meshes, because this method requires variables exactly on face centers, which are not generally obtained in a simple manner on Cartesian grids having hanging nodes (Fig. 1), for instance. Meanwhile, on thin-and-curved mesh that often appears in boundary-layers for high Reynolds number flow simulations, LSQ reportedly gives totally erratic gradients [1]; WLSQ with a properly chosen weighting function or G-G has better performance, albeit associated with certain errors, as shown in [5]. Therefore, each cell type/geometry has its own favorite gradient reconstruction methods, e.g., Cartesian grids prefer WLSQ to G-G, whereas thin-and-curved mesh does the opposite. Then, it is a natural question how to deal with mixed grids of different types of cells.

In recent years, body-fitted/Cartesian hybrid grids (or sometimes called viscous Cartesian grids) [4, 6-9] have been recognized as one of standard types of unstructured grids, because they can resolve boundary-layers as well as structured grids do, while saving the number of cells away from wall. Thus, in this study, we will propose a robust and (second-order) accurate hybrid reconstruction method of WLSQ and G-G suitable for, but not limited to, those mixed grids in a unified manner, which overcomes the above-mentioned difficulties encountered by existing

^{*} Senior Researcher and Director, JAXA's Engineering Digital Innovation (JEDI) Center, 3-1-1 Yoshinodai, Chuo, AIAA Member.

[†] Research Fellow of Japan Society for the Promotion of Science (JSPS), JAXA's Engineering Digital Innovation (JEDI) Center, 3-1-1 Yoshinodai, Chuo, AIAA Member (Corresponding Author); currently Assistant Professor at Nagoya University, Furo-cho, Chikusa-ku, Nagoya, Japan.

[‡] Researcher, JAXA's Engineering Digital Innovation (JEDI) Center, 3-1-1 Yoshinodai, Chuo, AIAA Member.

methods. Our discussions are based on cell-centered schemes, but extendable to the cell-vertex counterpart by simple replacement of the word “cell” with “control volume.”

We point out here that many CFD practitioners still desire second-order accuracy in space within the framework of an unstructured grid finite-volume-method (FVM) [10-13]. This has motivated us to pursue a second-order accurate reconstruction method applicable to wide-ranging grid types and/or geometries, in spite of growing attentions to more sophisticated, higher-order methods such as discontinuous Galerkin [14], spectral volume [15], or residual distribution [16, 17] in the past several years.

II. Governing Equations and Discretization

The governing equations are the compressible Euler equations, discretized for FVM and applied to a polyhedral computational cell i , sharing a face (i, j) with a neighboring cell j . The method can be directly applied to the inviscid component of the viscous computations. Our discussion is based on a cell-centered FVM, and an example of a two-dimensional cell is illustrated in Fig. 2; however, it also holds for a cell-vertex FVM when the word “cell” is simply replaced by the “control volume.” The inviscid flux can be computed by any numerical flux functions such as an approximate Riemann problem solver, and we chose an advection upstream splitting method (AUSM)-type scheme, simple low-dissipation AUSM (SLAU) [18] here, using physical quantities on both sides of the cell interface and face normal of the cell interface.

The cell interface values are extrapolated from the cell center values using the gradient as;

$$q_{i,j} = q_i + \phi_i \nabla q_i \cdot (\bar{x}_{i,j} - \bar{x}_i) \quad (2.1)$$

Here ϕ_i is a slope limiter [19-21] usually employed to suppress spurious oscillations at captured discontinuities such as a shock. In this work, however, we simply set $\phi_i=1$ because we focus on unlimited gradients and treat subsonic flows only. Lower-Upper Symmetric Gauss-Seidel implicit scheme [22] is employed for time integration.

III. Proposed Method #1: WLSQ (G)

A. WLSQ (G): Weight Function for WLSQ inherited from G-G

Features of G-G come from usage of cell face areas as appropriate weights for the center values of the surrounding cells. Thus, the weight function ω_{ij} , by which WLSQ has similar nature to G-G, is considered. From the gradient formula of WLSQ (N) [where $\omega_{ij} = L_{ij}^{-N}$ (L_{ij} : distance between cells i and j)] is coined WLSQ (N) here for

convenience; (Unweighted) LSQ is referred to as WLSQ (0) in this unified manner] and that of G-G, the weighting from a surrounding (j -th) cell, Δq_j , in each scheme has the following form:

$$\text{WLSQ: } \mathbf{M}^{-1} \omega_j L_j \bar{\mathbf{x}}_{L_j} \Delta q_j \quad \left(\because \mathbf{M} \nabla q = \sum_j \omega_j \Delta q_j \Delta \bar{\mathbf{x}}_j = \sum_j \omega_j L_j \Delta q_j (\bar{\mathbf{x}}_{L_j})_j \right) \quad (3.1a)$$

$$\mathbf{M} = \begin{pmatrix} I_{XX} & I_{XY} & I_{ZX} \\ I_{XY} & I_{YY} & I_{YZ} \\ I_{ZX} & I_{YZ} & I_{ZZ} \end{pmatrix}; \quad I_{AB} = \sum_j \omega_j \Delta A \Delta B \quad (3.1b)$$

$$\text{G-G: } \frac{1}{V_0} s_j \alpha_j \bar{\mathbf{x}}_{n_j} \Delta q_j \quad (3.1c)$$

where subscript i is omitted for brevity; $(\bar{\mathbf{x}}_{L_j})_j$ is the unit vector along $\Delta \bar{\mathbf{x}}_j$, defined as $(\bar{\mathbf{x}}_{L_j})_j = \Delta \bar{\mathbf{x}}_j / L_j$ where $\Delta \bar{\mathbf{x}}_j = \bar{\mathbf{x}}_j - \bar{\mathbf{x}}_i$, i.e., a direction vector from i -th to j -th cell center; A and B stand for x, y , or z ; V_0 is the volume of current cell; s_j is interface area; α_j is usually taken to be a half; $(\bar{\mathbf{x}}_{n_j})_j$ is the unit normal vector outward from the interface. If the mesh is nearly orthogonal, we have the following approximate relation

$$\bar{\mathbf{x}}_{n_j} \approx \bar{\mathbf{x}}_{L_j} \quad (3.2)$$

When we focus on the weight of j -th cell, the constant coefficients \mathbf{M}^{-1} and $1/V_0$ can be neglected. Therefore we can use the following weight function for WLSQ so that the similar weight from j -th cell in G-G is realized

$$\omega_j = \frac{\alpha_j s_j}{L_j} \quad (3.3)$$

Then, the interpolation factor α_j is defined to give second-order spatial accuracy in a one-dimensional case. This argument is also valid for parallel and linear meshes, even if they are non-orthogonal or non-uniform. When α_j is defined as

$$\alpha_{W_j} = \left(\frac{2l_j}{L_j} \right)^2 \quad (3.4)$$

where subscript ‘‘W’’ stands for ‘‘WLSQ,’’ and l_j is distance between the cell center and the face center (see Fig. 2).

The weight function using this factor becomes

$$\omega_j = \left(\frac{2l_j}{L_j} \right)^2 \frac{s_j}{L_j} = 4s_j l_j^2 L_j^{-3} \quad (3.5)$$

Consequently, it is equivalent with the weight function of WLSQ (3) which has second order spatial accuracy, considering s_j and l_j are constant in this 1D case. For a non-orthogonal cell, the Eq. (3.4) is extended using projections of L_j and l_j to cell-face normal, L_j' and l_j' (as illustrated in Fig.2) as:

$$\alpha_{w_j} = \left(\frac{2l_j'}{L_j'} \right)^2 \quad (3.6)$$

Finally, WLSQ using the following weight function is named as WLSQ (G)

$$\omega_j = \left(\frac{2l_j'}{L_j'} \right)^2 \frac{s_j}{L_j} \quad (3.7)$$

This WLSQ (G) preserves linear distribution and gives second-order spatial accuracy for a parallel linear mesh.

B. Treatment of Anisotropic Point Distribution

Two dimensional cells with hanging nodes shown in Fig. 3 are considered, as a practical example. Coordinates and value at point P_j are denoted as x_j and q_j , respectively. The edge length of the larger square is set as h , and weights of P_1 and P_2 are set as ω_a , and those of P_3 , P_4 and P_5 are set ω_b from the symmetry condition. The gradient in x direction using WLSQ is computed from Eq. (3.1) as

$$q_x = \left(\frac{9}{8}\omega_a + \omega_b \right)^{-1} \left(\frac{9}{8}\omega_a \frac{\frac{1}{2}(q_1 + q_2) - q_0}{\frac{3}{4}h} + \omega_b \frac{q_4 - q_0}{h} \right) \quad (3.8)$$

On the other hand, suppose two points P_1 and P_2 are represented by a single point P_T virtually sitting in their middle, and the value there is $(q_1 + q_2)/2$ (See Fig. 3). In this case, the x direction gradient calculated by WLSQ is shown below.

$$q_x = \left(\frac{9}{16}\omega_T + \omega_b \right)^{-1} \left(\frac{9}{16}\omega_T \frac{q_T - q_0}{\frac{3}{4}h} + \omega_b \frac{q_4 - q_0}{h} \right) \quad (3.9)$$

This gives second-order spatial accurate gradient for the x -direction, because the mesh is supposed to be parallel and linear in a 1D sense. Now it is found that Eq.(3.8) and Eq.(3.9) are equivalent, if the condition below is satisfied.

$$\omega_T = 2\omega_a \quad (3.10)$$

The weighting function of WLSQ (G) satisfies this condition because of cell-cell and cell-face distances considered in Eq. (3.6), whereas WLSQ (N) does not. Therefore, it is confirmed that anisotropy is properly treated in the proposed method.

C. Thin-and-curved Mesh

As stated earlier in [5], it is necessary to use WLSQ (2) in order to obtain robust gradients on thin-and-curved meshes, at the expense of nominal second-order accuracy. It is shown in this subsection that WLSQ (G) behaves as robustly as WLSQ (2) but with second-order accuracy retained as WLSQ (3) on such a cell. The following relations exist for the (two-dimensional) cell shown in Fig. 4.

$$\begin{aligned} s_1 = s_3 &\approx L_2 \\ s_2 &\approx s_4 \approx L_1 \\ V_o &\approx L_1 L_2 \end{aligned} \tag{3.11}$$

If these relations are used, the weighting function of WLSQ (G) become as follows

$$\begin{aligned} \omega_1 &= \frac{s_1}{L_1} \left(\frac{l_1'}{L_1'} \right)^2 \approx \frac{1}{4} \frac{L_2}{L_1} \approx \frac{1}{4} \frac{V_o}{L_1^2} \\ \omega_2 &= \frac{s_2}{L_2} \left(\frac{l_2'}{L_2'} \right)^2 \approx \frac{1}{4} \frac{L_1}{L_2} \approx \frac{1}{4} \frac{V_o}{L_2^2} \end{aligned} \tag{3.12}$$

where cell index i is omitted, again. Since constant factor $V_o/4$ can be neglected, these correspond with weights of WLSQ (2), and hence, WLSQ (G) behaves as WLSQ (2) in this case. Recall that both second-accuracy and robustness for thin cells cannot be realized at the same time when WLSQ (N) is used. On the other hand, WLSQ (G) has both virtues, because it behaves like WLSQ (2) on thin-and-curved meshes and WLSQ (3) elsewhere.

IV. Proposed Method #2: Green-Gauss/Weighted-Least-Squares (GLSQ)

A. GLSQ: Hybrid Formula of G-G and WLSQ (G)

It has been geometrically shown that WLSQ (G) should give reasonable gradients for all the meshes considered here. It will be numerically shown later in Sec. V-B, however, that all WLSQs including WLSQ (G) can exhibit huge reconstruction error on a thin-and-distorted mesh even if cell center gradient is calculated properly. On the other hand, G-G is more stable on such meshes. Thus, a mixed formula which switches between G-G and WLSQ is proposed. After introducing a dimensional consistency constant D , the formula is given as follows (again, subscript i is omitted for brevity).

$$[\beta_o \mathbf{M}_o + 2D(1-\beta_o)V_o \mathbf{I}] \nabla q_o = \beta_o \sum_j \omega_j L_j \Delta \bar{x}_{L_j} \Delta q_j + 2D(1-\beta_o) \sum_j \alpha_{G_j} s_j \bar{x}_{n_j} \Delta q_j, \quad (4.1)$$

$$\beta_o \in [0,1]$$

This formula gives G-G when $\beta_o=0$, and WLSQ when $\beta_o=1$. If WLSQ (G) is used as the WLSQ, the constant D can be simply taken as unity. Finally, the following method, named GLSQ (G-G/WLSQ), is obtained.

$$[\beta_o \mathbf{M}_o + 2(1-\beta_o)V_o \mathbf{I}] \nabla q_o = \sum_j (\beta_o \alpha_{W_j} \bar{x}_{L_j} + 2(1-\beta_o) \alpha_{G_j} \bar{x}_{n_j}) s_j \Delta q_j \quad (4.2)$$

GLSQ needs inversion of the 3×3 matrix, and the right hand side is slightly complex. However, increase of computational cost is trivial, if the matrix is once set and inverted before flow simulations for a time-independent mesh. Small interpolation parameter β_o is expected to be used on thin-and-distorted cells, leading to G-G. The actual method to set β_o will be mentioned in the next subsection.

B. Geometrical Monotonicity Condition and Definition of Parameter β_o

It will be shown here that a kind of monotonicity condition, which depends only on mesh geometry, has to be satisfied when the robustness of CFD scheme is considered. The difference between cell interface value and cell center value can be expressed by linear combination of finite difference of cell center values as follows in both WLSQ and G-G.

$$q_{i,j} - q_i = \sum_j C_{ij} \Delta q_j \quad (4.3)$$

For example, the coefficient matrix C_{ij} of GLSQ is expressed as follows.

$$C_{ij} = (\bar{x}_{i,j} - \bar{x}_i) \cdot [\beta_o \mathbf{M}_o + 2(1-\beta_o)V_o \mathbf{I}]^{-1} \sum_j (\beta_o \alpha_{W_j} \bar{x}_{L_j} + 2(1-\beta_o) \alpha_{G_j} \bar{x}_{n_j}) s_j \quad (4.4)$$

Also the coefficient matrix of G-G is expressed as

$$C_{ij} = (\bar{x}_{i,j} - \bar{x}_i) \cdot \frac{(s \bar{x}_n)_j}{2V_o} \quad (4.5)$$

where $\alpha_G=1/2$ is assumed. Here, the coefficient matrix is required to satisfy monotonicity condition as

$$|C|_{\max} \equiv \max(|C_{ij}|) < 1 \quad (4.6)$$

This is equivalent to the condition below when only $(q_{i,j} - q_i)$ has non-zero value and difference in values to other cells are all zero: such a situation can occur at initial step on solid wall boundaries.

$$|q_{i,j} - q_i| < |\Delta q_j|, \forall i,j \quad (4.7)$$

If this condition is not satisfied, unphysical new extrema can be generated, leading to blow-up of the flow computation. For example, in case of second order central difference scheme on a smooth mesh, the following is usually satisfied:

$$|C|_{\max} \approx 0.25 \quad (4.8)$$

The absolute value of coefficient matrix of G-G expressed by Eq. (4.5) is also smaller than unity for convex cells. Therefore, the geometric monotonicity is not violated in finite difference scheme and G-G. On the other hand, sometimes huge violations are found in WLSQ as will be stated later in Sec. V-B. It can be illustrated as follows. It is not direct conjunction, however, the contribution from cell “ j ” in WLSQ tends to enhance the gradient in \bar{x}_L direction as expressed in Eq.(3.1a) (See Fig. 5). Then, this gradient tends to make the difference between cell center and cell face larger as

$$q_{i,j} - q_i = \bar{x}_{Lj} \cdot (\bar{x}_{i,j} - \bar{x}_i) \Delta q_j \quad (4.9)$$

When the cell is not orthogonal and its aspect ratio is large, the inner product in (4.9) can be very large. In G-G, on the other hand, the contribution from cell “ j ” enhances the gradient in \bar{x}_n direction, and $(\bar{x}_{nj}, (\bar{x}_{i,j} - \bar{x}_i))$ will never become so large in convex cells. Then the value of interpolation parameter β_o is set to satisfy this monotonicity condition expressed by Eq. (4.6). If $\beta_o \ll 1$ is assumed, Eq. (4.4) is expanded with the first order approximation with regard to β_o as

$$C_{ij} \approx (\bar{x}_{i,j} - \bar{x}_i) \cdot \frac{s_j}{2V_o} \left\{ \bar{x}_n + \beta_o \left(\alpha_{wi} \bar{x}_i - \frac{1}{2V_o} \mathbf{M}_o \bar{x}_n \right) \right\}_j \quad (4.10)$$

where $\alpha_G=1/2$ is assumed again. Thus, the following sufficient condition can be derived.

$$\beta_o < \min \left(\frac{\left| \frac{2V_o}{s_j} - \left| \bar{x}_{ni} \cdot (\bar{x}_{i,j} - \bar{x}_i) \right| \right|}{\left| \left(\alpha_{wi} \bar{x}_{Li} - \frac{1}{2V_o} \mathbf{M}_o \bar{x}_{ni} \right) \cdot (\bar{x}_{i,j} - \bar{x}_i) \right|} \right) \quad (4.11)$$

The uncertainty of matrix \mathbf{M} makes definition of β_o non-trivial, but the following approximate relation can be used in WLSQ (G), when the monotonicity violation occurs.

$$\text{Numerator} \approx \frac{2V_o}{s_j} \quad (4.12a)$$

$$\text{Denominator} < |\bar{x}_{i,j} - \bar{x}_i| \quad (4.12b)$$

Considering these, the following simple definition is found sufficient for the hybrid meshes through our numerical experiments.

$$\beta_o = \min\left(1, \frac{2}{AR}\right), \quad AR \equiv \frac{2 \cdot \max|\bar{x}_{i,j} - \bar{x}_i| \cdot \max(s_j)}{V_o} \quad (4.13)$$

where AR has been defined as an “effective” aspect ratio for arbitrary polyhedra and polygons, meaning (*Maximum Side Length*)/(*Minimum Side Length*), if, for instance, (2D) uniformly spaced rectangular cells are considered: the full WLSQ (G) is used in cells whose AR s are smaller than 2, and GLSQ asymptotes to G-G in higher aspect ratio cells. Therefore, the WLSQ (G) is used in the Cartesian mesh portion of the hybrid mesh system whereas G-G is used in the part of layer cells.

V. Numerical Examples

We will put a simple function upon each cell in the first example and compare numerical and analytical solutions; in the second case, we will discuss monotonicity of each method and its relation to cell geometrical properties; in the final example, we will solve Euler equations on a subsonic flow around a two-dimensional airfoil.

A. Simple Function on Triangular and Quadrilateral Meshes around Cylinder

In order to compare the accuracy of the methods, a simple function for a simple geometry is numerically differentiated. The function $q=r^2$ is numerically set on meshes around a two dimensional circular cylinder having unit radius, and q_r , a radial directional derivative of q , is computed using the several methods based on a cell-centered FVM. Then, they are compared with the exact value, i.e. $q_r=2r$. Quadrilateral [$(AR)_{\max} = 628$] and triangular [$(AR)_{\max} = 838$] meshes shown in Fig. 6 (coarse) are used. The detailed mesh information is expanded in Table 1. The methods used are G-G; WLSQ (0); WLSQ (1); WLSQ (2); WLSQ (3) which has the second-order spatial accuracy in linear meshes; and WLSQ (G) presented in this paper. Figure 7 shows the numerical errors from the analytical solution versus distance R from cylinder center (i.e., $R=1$ corresponds to cylinder surface). The results in Fig. 7 are summarized as:

- G-G gives a reasonable solution for the quadrilateral mesh (1% error), but around 10% error in the triangular mesh even away from the wall. This is because the geometrical assumption that the face center be located in the middle of two cell centers is invalid in the triangle mesh.
- WLSQ (0) exhibits huge error (up to 100%) in both cases, because it gives $q_r \approx 0$ near the body.

- WLSQ (3) gives the best accuracy in the quadrilateral mesh (less than 0.1%), but shows huge error (up to 100%) in the triangular mesh near the wall.
- WLSQ (G) shows overall satisfactory accuracy in both cases: 0.1% error in the quadrilateral mesh; and 0.1 % in the portion away from the wall and less than 10% error near the wall in the triangle mesh.

In addition, we confirmed that a different mesh spacing showed qualitatively the same profiles. Thus, the errors only at the inner-most cells (i.e., wall-neighbor cells) versus their sizes are compared in Fig. 8:

- All the methods except for WLSQ (0) show the nominal second order accuracy on the quadrilateral mesh.
- On the triangular mesh, on the other hand, only WLSQ (G) achieved the second order, and the others are at most first order accurate.

Thus, from the accuracy point of view, WLSQ (G) seems the best among those above. Note that the GLSQ solution must fall between WLSQ (G) (away from the wall – second order) and G-G (near the wall – first order) results. Furthermore, we confirmed that those findings are consistent with the results for a simpler, linear $q=r+1$ function.

B. Geometrical Monotonicity Assessment

The geometrical monotonicity stated above in Sec. IV-B is investigated for hybrid meshes having thin-layer cells around a sphere and an airfoil, as shown in Figs. 1 and 9, respectively. The maximum values of $|C|_{i,j}$ defined by Eqs. (4.4-6) in each computational space are shown in Table 2, along with maximum AR s of $O(10^3)$ defined in Eq. (4.13) (and the minimum AR is of course 1 in the Cartesian region in each grid). We remind again that it is necessary to keep $|C|_{\max}$ smaller than unity for monotonicity. However, this is satisfied only by WLSQ (0), G-G, and GLSQ, whereas WLSQs (1-3) and WLSQ (G) show significant violations. Remembering the fact that WLSQ (0) cannot compute proper gradients in thin meshes and gives too small gradient there, monotonicity of WLSQ (0) is realized only because of its low accuracy. Therefore, only G-G and GLSQ are acceptable in terms of both monotonicity and accuracy; all WLSQs including WLSQ (G) except for WLSQ (0) can generate unphysical values in thin cells and may blow up the computation. This unphysical peak may be practically suppressed by applying a slope limiter in expense of accuracy. In Table 3, all the methods treated here are summarized.

C. Flow computations around Two-Dimensional Airfoil using Hybrid Mesh

An inviscid flow around the two-dimensional NACA0012 airfoil (both the chord and spanwise lengths are 1) at Mach 0.3 and 0 angle of attack is computed using a 3D hybrid mesh [380,000 cells; highest effective aspect ratio is

$(AR)_{\max} = 4667.7]$ shown in Fig. 9. G-G, WLSQ (0), and GLSQ (without a slope limiter) are used to calculate gradients, and SLAU [18] is used as a numerical flux function. We point out that it was actually necessary to use a slope limiter for WLSQ (2) in this problem involving cells with ARs of $O(10^3)$, because of its geometrical monotonicity violation as demonstrated in the previous subsection – hence, the WLSQ (2) result is omitted.

It is known that a two dimensional object mounted in an inviscid and subsonic flow has no drag in theory, thus, the amount of drag produced by a numerical computation is a good indicator of overall numerical errors. Since the magnitude of drag varies with mesh fineness, only relative comparison is worth doing, as done in Fig. 10 for different reconstruction methods. It is clearly seen that the GLSQ, which can keep linear distributions in the outer Cartesian mesh and give proper gradients in the layer mesh, shows lower error than others do. Figure 11 shows entropy distributions defined by $\ln\left\{\frac{p/\rho^\gamma}{(p_\infty/\rho_\infty^\gamma)}\right\}$ (theoretically zero, again) around leading edges and trailing edges on the center plane, $z=0.5$. It is confirmed that GLSQ, again, shows the smallest entropy generation near the airfoil, as clearly seen in layer cells where ARs are large. To verify the developed method, a grid convergence study is conducted and reported in Appendix. A.

VI. Conclusions

By combining the strengths of G-G (Green-Gauss) and WLSQ (weighted-least-squares) formula, new gradient reconstruction methods for unstructured meshes are presented. First, the weight function of WLSQ is obtained from the analogy of G-G [as the first method, WLSQ (G)]; second, WLSQ (G) and G-G are smoothly switched using a blending function based on the geometry of each cell, as GLSQ (Green-Gauss/Weighted-Least-Squares). Both WLSQ (G) and GLSQ achieve satisfactory accuracy in geometrical and computational viewpoints.

The geometrical monotonicity condition, which should be satisfied by a gradient calculation method for robustness, is also introduced and discussed. It is shown that only G-G and GLSQ satisfy this condition. It suggests that gradient computed by the other methods should be used with some slope limiter for robustness even if flows are smooth. Overall, GLSQ shows the best performance in terms of both accuracy and robustness, as expanded below:

- Second-order spatial accuracy for cell center gradient in linear grid systems, and nearly second-order otherwise
- Exact value for linear distribution except for a very thin mesh
- Reasonable gradient in a very thin mesh which most of WLSQ fails to compute
- As simple a formulation as conventional WLSQ

Furthermore, improved, unique derivation of face-center coordinates has also been proposed and used with success.

Acknowledgments

This work is partly supported by JSPS (Japan Society for the Promotion of Science). The unstructured grid generation tool “LS-GRID” and the solver “LS-FLOW” used in flow computations were developed by Keiichiro Fujimoto and Kazuto Kuzuu with the authors at JEDI center, JAXA, Japan. Z.J. Wang at Iowa State University and Junya Aono at Research Center of Computational Mechanics, Inc., Japan, helped us developing those codes. We are grateful to all their cooperation.

References

- [1] Mavriplis, D.J., “Revisiting the Least-Squares Procedure for Gradient Reconstruction on Unstructured Meshes,” AIAA Paper 2003-3986, 2003.
- [2] Wang, Z.J., “A Fast Nested Multi-Grid Viscous Flow Solver for Adaptive Cartesian/Quad Grids,” *Int. J. Numer. Meth. Fluids*, Vol. 33 (2000), pp.657-680.
- [3] Aftosmis M., Gaitonde D, Tavares TS, “On the accuracy, stability and monotonicity of various reconstruction algorithms for unstructured meshes”, AIAA Paper 94-0415, 1994.
- [4] Hirsch, C., “Numerical Computation of Internal and External Flows, Volume 1, Second Edition: The Fundamentals of Computational Fluid Dynamics,” Butterworth-Heinemann, Burlington, 2007.
- [5] Shima, E., Kitamura, K., and Fujimoto, K., “New Gradient Calculation Method for MUSCL Type CFD Schemes in Arbitrary Polyhedra,” AIAA Paper 2010-1081, 2010.
- [6] Wang, Z.J., and Chen, R.F., “Anisotropic Solution-Adaptive Viscous Cartesian Grid Method for Turbulent Flow Simulation,” *AIAA J.*, Vol. 40 (2002), pp.1969-1978.
- [7] Aftosmis, M.J., Berger, M.J., and Alonso, J.J., “Applications of a Cartesian Mesh Boundary-Layer Approach for Complex Configurations,” AIAA Paper 2006-0652, 2006.
- [8] Luo, H., Spiegel, S., and Lohner, R., “Hybrid Grid Generation Method for Complex Geometries,” *AIAA J.*, Vol.48 (2010), pp. 2639-2647. doi:10.2514/1.J050491
- [9] Hashimoto, A., Murakami, K., Aoyama, T., Ishiko, K., Hishida, M., Sakashita, M., and Lahur, P.R., “Toward the Fastest Unstructured CFD Code “FaSTAR”,” *50th AIAA Aerospace Sciences Meeting including the New Horizons Forum and Aerospace Exposition*, AIAA Paper 2012-1075, 2012.
- [10] Gnoffo, P., Buck, G., Moss, J., Nielsen, E., Berger, K., Jones, W.T. and Rubavsky, R., “Aerothermodynamic Analyses of

Towed Ballutes,” AIAA Paper 2006-3771, 2006.

- [11] Pandya, S., Onufer, J., Chan, W., and Klopfer, G., “Capsule Abort Recontact Simulation,” NAS Technical Report, NAS-06-005, 2006.
- [12] Catalano, P., Marini, M., Nicoli, A. and Pizzicaroli, A., “CFD Contribution to the Aerodynamic Data Set of the Vega Launcher,” *J. Spacecraft and Rockets*, Vol. 44 (2007), pp.42-51.
- [13] Bigarella, E.D.V., Azevedo, J.L.F. and Scalabrin, L.C., “Centered and Upwind Multigrid Turbulent Flow Simulations of Launch Vehicle Configurations,” *J. Spacecraft and Rockets*, Vol. 44 (2007), pp.52-65.
- [14] Cockburn, B., and Shu, C.W., “The Runge–Kutta Discontinuous Galerkin Method for Conservation Laws V: Multidimensional Systems,” *J. Comput. Phys.*, Vol. 141 (1998), pp.199–224.
- [15] Wang, Z.J., Zhang, L, and Liu, Y., “Spectral (Finite) Volume Method for Conservation Laws on Unstructured Grids IV – Extension to Two-Dimensional Systems,” *J. Comput. Phys.*, Vol. 194 (2004), pp.716-741.
- [16] Van Leer, B., “Upwind and High-Resolution Methods for Compressible Flow: From Donor Cell to Residual-Distribution Schemes,” *Commun. Comput. Phys.*, Vol. 1 (2006), pp.192-206.
- [17] Nishikawa, H., “A First-order System Approach for Diffusion Equation. I: Second-order Residual-Distribution Schemes” *J. Comput. Phys.*, Vol. 227 (2007), pp.315–352. doi:10.1016/j.jcp.2007.07.029
- [18] Shima, E. and Kitamura, K., “Parameter-Free Simple Low-Dissipation AUSM-Family Scheme for All Speeds,” *AIAA J.*, Vol. 49 (2011), pp.1693-1709. doi:10.2514/1.55308
- [19] Barth, T.J., and Jespersen, D.C., “The Design and Application of Upwind Schemes on Unstructured Meshes,” AIAA Paper 89-0366, 1989.
- [20] Venkatakrishnan, V., “Convergence to Steady State Solutions of the Euler Equations on Unstructured Grids with Limiters,” *J. Comput. Phys.*, Vol. 118 (1995), pp.120-130.
- [21] Kitamura, K., and Shima, E., “Simple and Parameter-Free Second Slope Limiter for Unstructured Grid Aerodynamic Simulations,” *AIAA J.*, , Vol. 50, No. 6 (2012), pp.1415-1426. doi:10.2514/1.J051269.
- [22] Jameson, A. and Turkel, E., “Implicit Schemes and LU Decompositions,” *Mathematics of Computation*, Vol. 37 (1981), pp. 385-397.

Appendix

A. Grid Study of Two-Dimensional Airfoil

The grid study of 2D airfoil case in Sec. V-C has been conducted. Since the original 3D grid already had many cells, we used the corresponding, genuinely 2D grid instead (extracted from the cross-section at $z=0.5$) as the “baseline” grid, and its refined version (“fine”). As summarized in Table A1, GLSQ achieved smaller drag

coefficients on the baseline and fine grids both: Thus, the grid convergence has been confirmed.

Figures

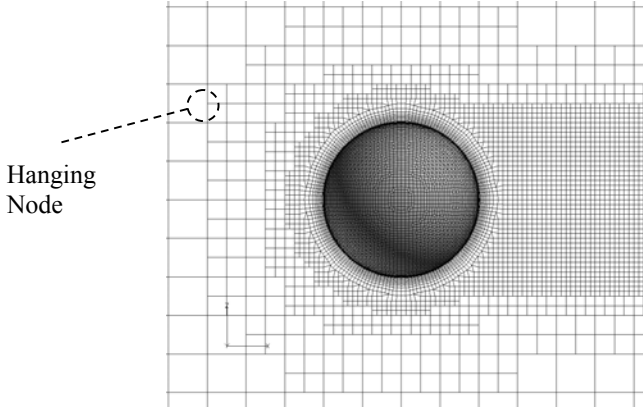


Figure 1. Hybrid mesh around a sphere.

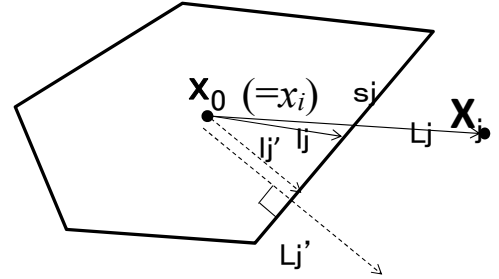


Figure 2. Schematic of cell geometrical values of a two-dimensional, arbitrary polygonal cell.

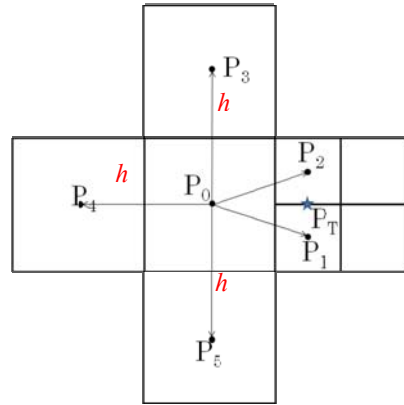


Figure 3. Anisotropy of point distribution for square mesh including hanging nodes.

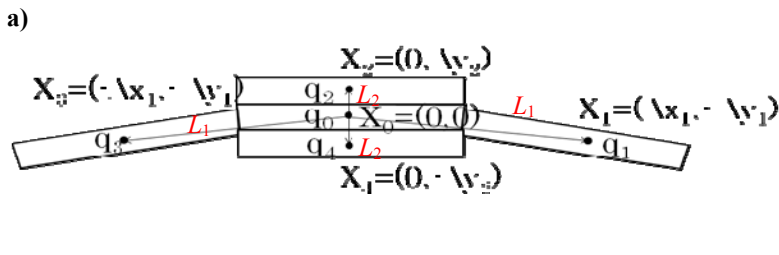


Figure 4: Example of distorted meshes, (a) vertically thin-and-curved case; (b) horizontally thin-and-distorted case.

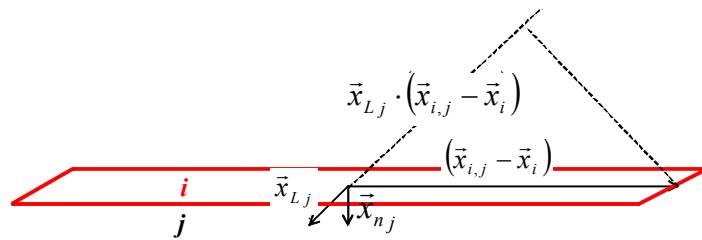


Figure 5. Illustration of huge reconstruction error caused by cell geometry.

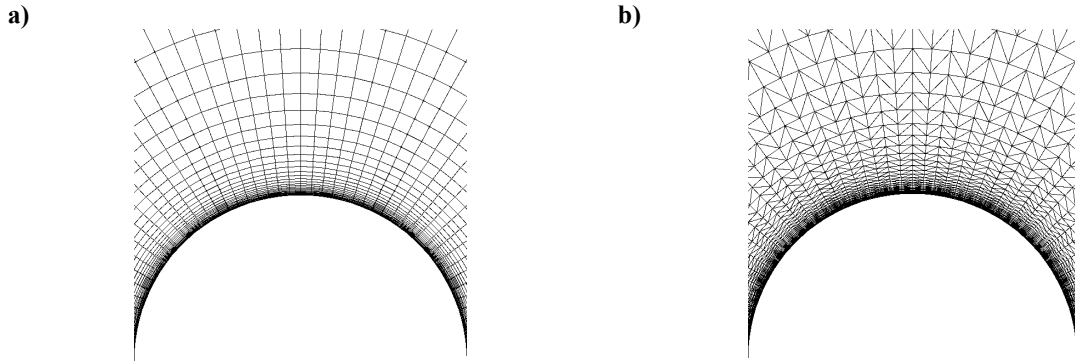


Figure 6: Quadrilateral (left) and triangular (right) baseline meshes around two-dimensional circular cylinder.

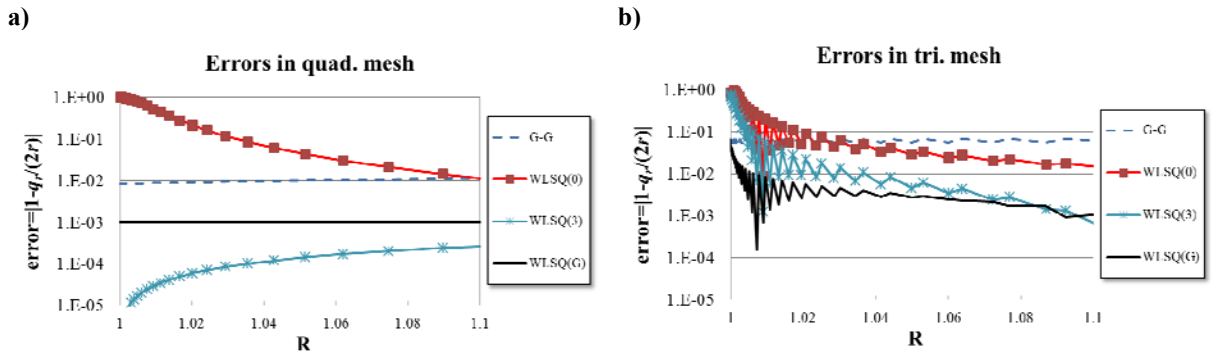


Figure 7: Errors to the exact values of each method, a) quadrilateral (baseline) mesh; and b) triangular (baseline) mesh.

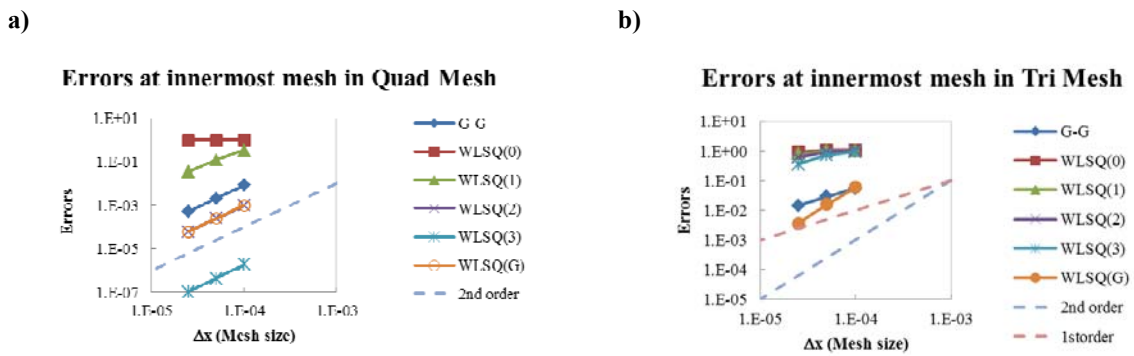


Figure 8: Errors (at innermost, i.e., wall-neighbor cells) vs. mesh sizes, a) quadrilateral mesh; and b) triangular mesh.

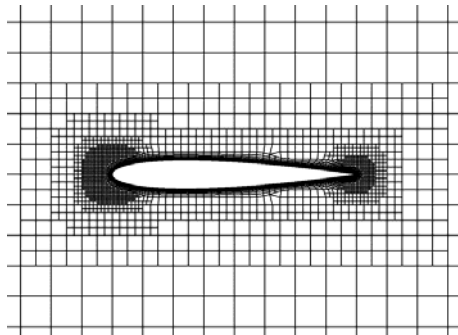


Figure 9: Grid around an airfoil (380,000 cells, displayed on center plane, $z=0.5$).

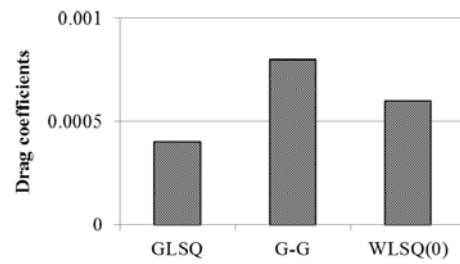


Figure 10: Comparison of drag coefficients by several reconstruction methods (theoretical drag is zero for this case, thus, lower drag indicates less error).

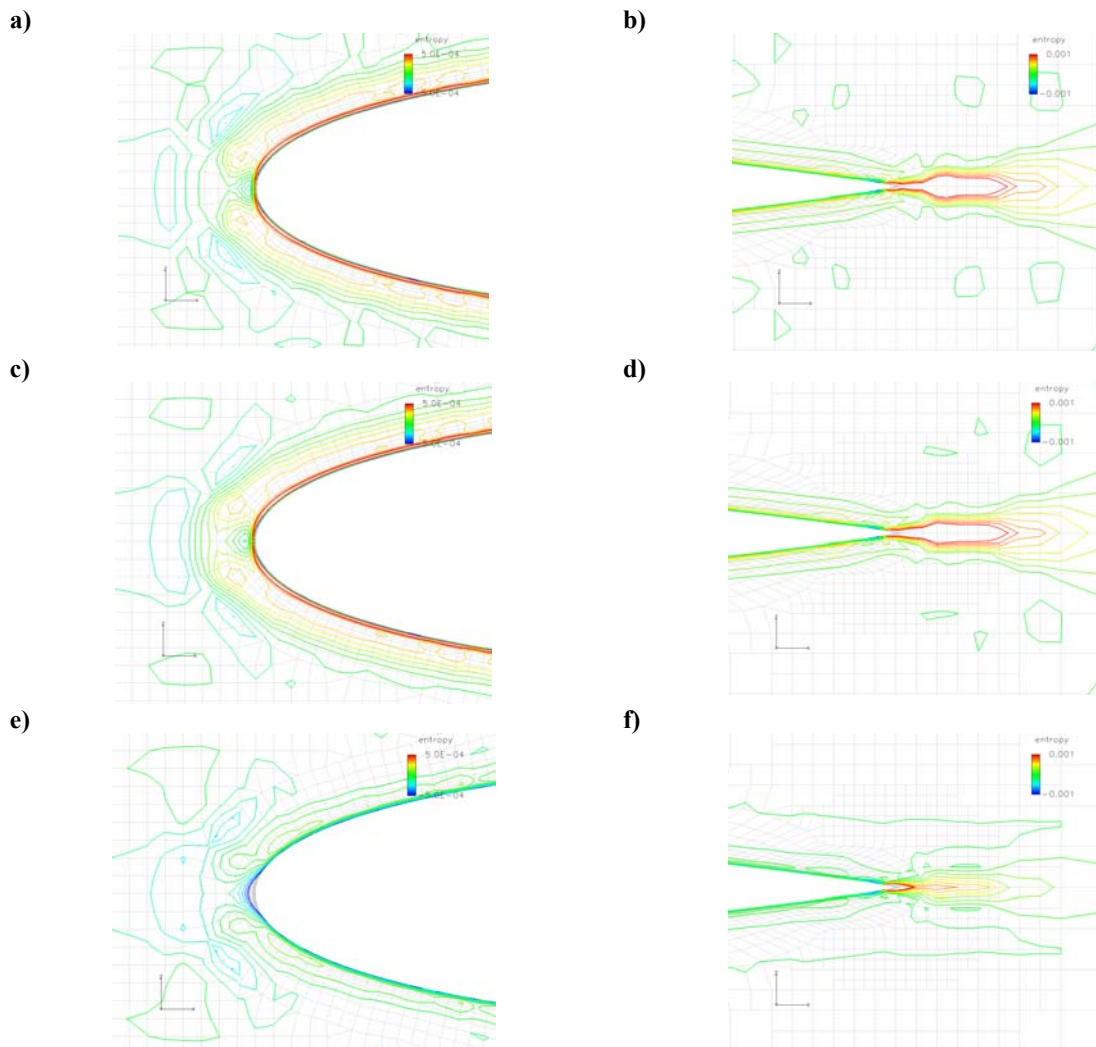


Figure 11. Comparison of entropy distribution of the inviscid subsonic flow around NACA0012 airfoil (on center plane, $z=0.5$). (a) G-G (leading edge), (b) G-G (trailing edge), (c) WLSQ (0) (leading edge), (d) WLSQ (0) (trailing edge), (e) GLSQ (leading edge), and (f) GLSQ (trailing edge)

Tables

Table 1. (Quadrilateral) Mesh Information around Circular Cylinder [Note: Triangular Mesh is generated simply by diagonally splitting each cell of corresponding Quadrilateral Mesh]

Grid Density	Minimum Spacing	Outward Grid Spacing Ratio	Radial Cells	Circumferential Cells
Coarse	1.0e-4	1.2	100	50
Baseline	5.0e-5	1.095	200	100
Fine	2.5e-5	1.046	300	200

Table 2. Maximum value of $|C|_{\max}$ in computational space for hybrid meshes around a sphere and an airfoil.

Gradient Reconstruction	Sphere [$(AR)_{\max} = 3004.5$]	Airfoil [$(AR)_{\max} = 4667.7$]
WLSQ(0)	0.971	0.442
WLSQ(1)	3.031	4.156
WLSQ(2)	445	253
WLSQ(3)	58418	18469
G-G	0.443	0.556
WLSQ(G)	553	290
GLSQ	0.606	0.517

Table 3. Properties of gradient reconstruction methods [* Criterion here is whether spatially second-order accuracy is theoretically achieved both on thin-and-curved meshes and Cartesian meshes having hanging nodes; ** Monotonicity of WLSQ (0) is only due to its low accuracy].

Gradient Reconstruction	Accuracy*	Monotonicity
WLSQ(0)	No	Yes**
WLSQ(1)	No	No
WLSQ(2)	No	No
WLSQ(3)	Yes	No
G-G	No	Yes
WLSQ(G)	Yes	No
GLSQ	Yes	Yes

Table A1. 2D Airfoil Grid Study Cases [$(AR)_{\max} = 3166$]

Grid Density	Minimum Spacing	No. of Total Cells	No. of layers in body-fitted grid	Cd (G-G)	Cd (GLSQ)
Baseline	1.0e-5	8,994	45	0.967e-3	0.697e-3
Fine	5.0e-6	26,774	75	0.641e-3	0.440e-3